Electronic structures of lead iodide based low-dimensional crystals

T. Umebayashi* and K. Asai†
Department of Quantum Engineering and Systems Science, The University of Tokyo, 7-3-1 Hongo, Bunkyo-ku, Tokyo, Japan and CREST, Japan Science and Technology Corporation, Tokyo, Japan

T. Kondo
Department of Materials Engineering, The University of Tokyo, 7-3-1 Hongo, Bunkyo-ku, Tokyo, Japan and CREST, Japan Science and Technology Corporation, Tokyo, Japan

A. Nakao
The Institute of Physical and Chemical Research, Hirosawa, Wako-shi, Saitama, Japan
(Received 23 July 2002; published 15 April 2003)

The electronic structures of three-dimensional and two-dimensional lead-halide-based crystals $CH_3NH_3PbI_3$ and $(C_4H_9NH_3)_2PbI_4$ are investigated by photoelectron spectroscopy and band calculations using the linear combination of atomic orbitals within the density-functional theory. For both crystals, the top of the valence band is found to consist mainly of the σ-antibonding states of Pb 6*s* and I 5*p* orbitals, and the bottom of the conduction band to be composed primarily of the σ-antibonding states of Pb 6*p* and I 5*s* orbitals. Photoelectron spectra of the valence-band region indicate that the electronic structures change depending on the dimensionality of the crystals. Based on the calculation results, the differences observed in the spectra are rationalized in terms of narrowing bandwidth as the dimensionality decreases from three to two dimensions. It is shown that the bandwidth narrowing of the two-dimensional crystal is due to zero dispersion in the vertical direction and the Jahn-Teller effect in the layered structure. These effects lead to a wideband gap and high exciton stability in $(C_4H_9NH_3)_2PbI_4$.

DOI: 10.1103/PhysRevB.67.155405 PACS number(s): 73.90.+f

I. INTRODUCTION

The physical properties of low-dimensional (LD) compounds have been investigated extensively because of the unique phenomena that occur when interactions between quanta (electrons, phonons, excitons, etc.) are confined to zero, one, or two dimensions. The large family of lead-iodide-based organic-inorganic perovskite compounds (OIPC's) has also attracted much attention as a series of unique optical LD materials.[1,2] OIPC's naturally form an LD quantum confinement structure of lead-iodide octahedra $[PbI_6]^{-4}$ and organic alkylammonium chains. These self-organizing processes result in extremely precise confinement structures on the angstrom order. This new class of materials exhibits remarkable excitonic and optical properties dependent on the dimensionality.[2–6] In particular, the excitonic and optical properties of two-dimensional(2D) single-layered OIPC's $(C_nH_{2n-1}NH_3)_2PbI_4$ $(n=4-12)$ have been examined extensively. Due to the quantum and dielectric confinement effects,[7] excitons are tightly confined in the lead-iodide layers. These materials, consequently, have large binding energies ($\sim$400 meV) and oscillator strength ($\sim$0.7 per formula unit) compared to the three-dimensional OIPC's $CH_3NH_3PbI_3$.[3–6]

Even though the effects of dimensionality on the excitonic and optical properties of OIPC's are a frequent topic of investigation, there have been few reports regarding the electronic structures of OIPC's. One notable exception is the work of Papavassiliou,[8] who has analyzed the electronic structures of OIPC's using band calculations by a semiempirical method based on the extended Hückel theory,[9] and a first-principles approach based on the Hartree-Fock theory.[10] Those researchers estimated the theoretical binding energies of excitons in three-, two-, one-, and zero-dimensional OIPC's from the semiempirical calculation results. However, there remains much work still to be done on the electronic structures of OIPC's.

In the present study, the authors focus on the effect of dimensionality on the electronic structures of the lead-iodide-based OIPC's $CH_3NH_3PbI_3$ (3D) and $(C_4H_9NH_3)_2PbI_4$ (2D). The electronic structures are investigated by ultraviolet photoelectron spectroscopy (UPS), and first-principles band calculations are performed to aid the discussion related to dimensional effects.

II. METHODS

A. Experiments

In the UPS measurements, polycrystalline thin films of OIPC's on silicon (Si) substrates were used to prevent the sample from electrostatic charging. OIPC's were synthesized in a nitrogen gas atmosphere. Stoichiometric amounts of PbI_2 and CH_3NH_3I (3D) or $C_4H_9NH_3I$ (2D) were dissolved in acetone, and the solution was spin coated onto the Si substrates. X-ray-diffraction (XRD) patterns, photoluminescence spectra, and atomic force microscopy (AFM) images confirmed that the thin films formed on the substrate were polycrystalline OIPC's. UPS measurements were carried out at room temperature using a THERMO VG ESCALAB 250 spectrometer with helium I resonance lamp ($\hbar\omega = 21.2$ eV).

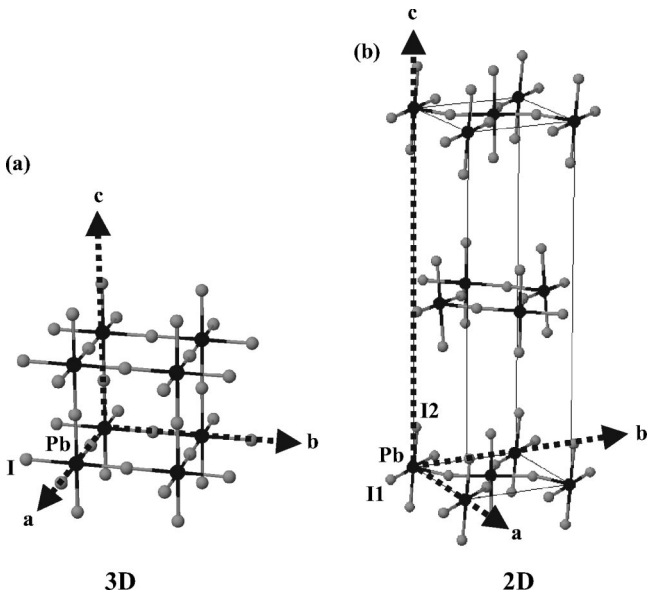

FIG. 1. Crystal structures of inorganic parts of (a) 3D crystal $CH_3NH_3PbI_3$ and (b) 2D crystal $(C_4H_9NH_3)_2PbI_4$. In-plane I atoms and out-of-plane I atoms are labeled I1 and I2, respectively.

B. Calculation

The linear combination of atomic orbitals (LCAO) self-consistent-field method implemented in the CRYSTAL98 code[11] was employed to calculate the 3D and 2D electronic structures. The calculations were based on the density-functional theory[12] (DFT) with the generalized-gradient approximation.[13,14] As all-electron basis sets are not practical from a computational point of view, the effective-core potential was used for the inner shells of Pb and I atoms.[15,16] The Gaussian basis sets adopted to describe Pb and I atoms have already been described in the studies of PbF_2 (Ref. 17) and

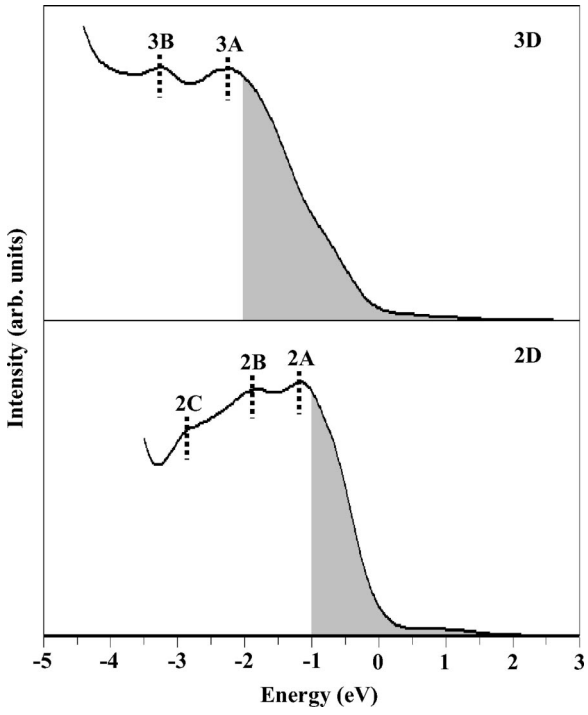

FIG. 2. UPS spectra of (a) 3D crystal $CH_3NH_3PbI_3$ and (b) 2D crystal $(C_4H_9NH_3)_2PbI_4$. Upper edge of the VB was set to zero for the initial-state energy.

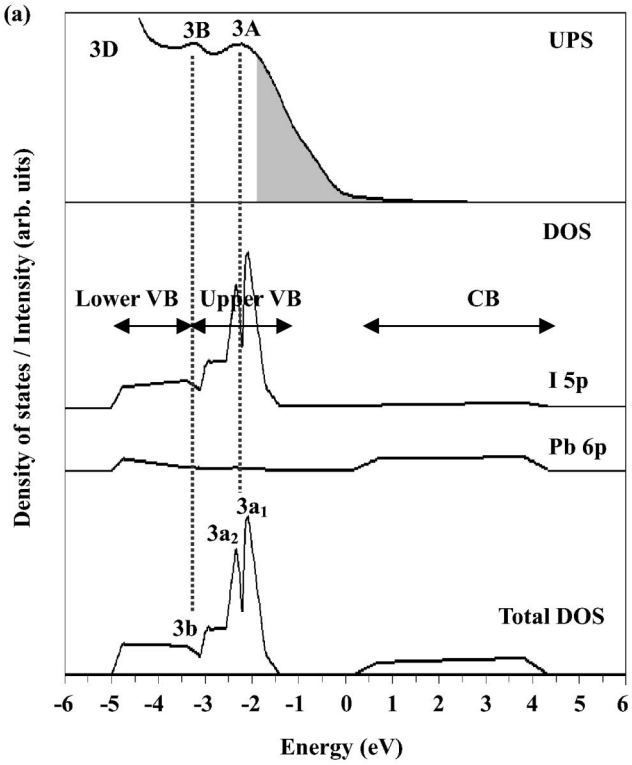

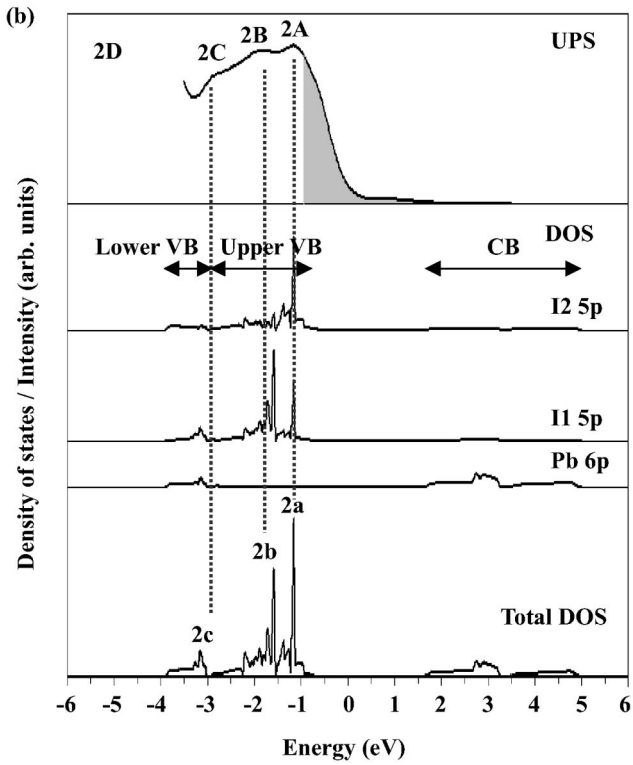

FIG. 3. UPS spectra of (a) 3D crystal $CH_3NH_3PbI_3$ and (b) 2D crystal $(C_4H_9NH_3)_2PbI_4$. Upper edge of the VB was set to zero for the initial-state energy.

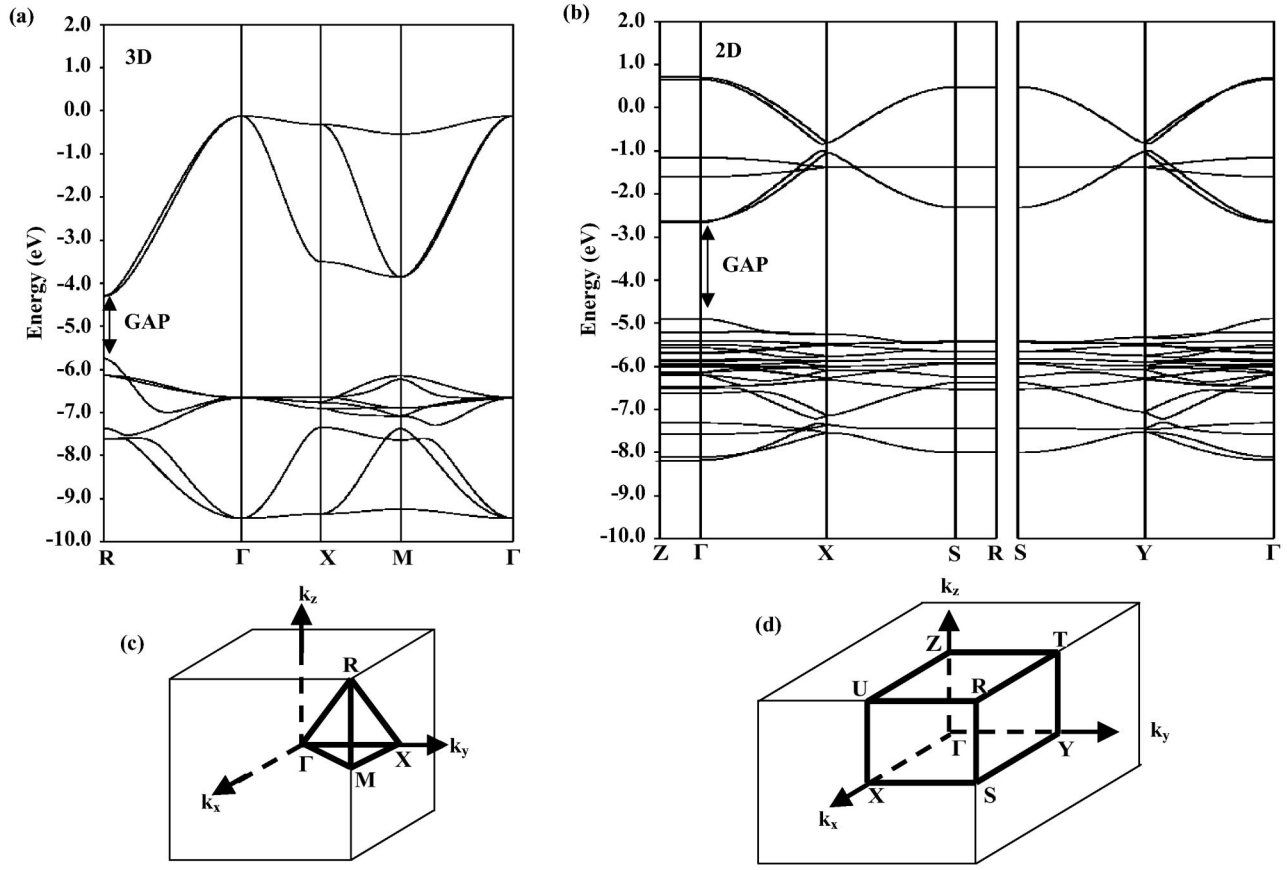

FIG. 4. Calculated band structures of (a) 3D crystal $CH_3NH_3PbI_3$ and (b) 2D crystal $(C_4H_9NH_3)_2PbI_4$ along the high-symmetry lines in the first Brillouin zone. The first Brillouin zone of the 3D and 2D crystals are indicated in (c) and (d).

LiI.[18] The exponents of the most diffuse *sp* shells of each atom were optimized by searching for the minimum total crystalline energy of the 3D structure corresponding to the published XRD data.[19]

Figure 1 shows the crystal structures of the inorganic parts of the OIPC's. The structural data have been reported previously.[19,20] The space group of the 3D and 2D crystals are $Pm3m$ and $Pbca$, respectively, with one (3D crystal) or four (2D crystal) formula units in the unit cell. Because the OIPC's have disordered alkylammonium chains $(C_nH_{2n-1}NH_3^+)$ with many different orientations, it is difficult to determine the crystal structures of the organic parts with high accuracy by x-ray-diffraction measurements. Based on the previous studies,[1–5,21,22] we can assume that the remarkable excitonic, optical, and electronic properties are attributed exclusively to the low-dimensional inorganic parts, the $[PbI_6]^{-4}$ network. Therefore, $C_nH_{2n-1}NH_3^+$ was ignored in the calculations, and a uniform background charge density was added to neutralize the charge in the unit cell.[23]

III. RESULTS AND DISCUSSION

A. UPS spectra and density of states

Figure 2 shows UPS spectra for the 3D and 2D samples in the valence-band (VB) region. In the spectra, the zero of the initial-state energy is located at the upper edge of the VB. Two peaks, $3A$ and $3B$, are observed in the spectrum for the 3D sample, whereas three peaks, $2A$, $2B$, and $2C$, appear in the 2D spectrum. As indicated by the shaded region, the spectral shapes of the upper VB clearly differ between these two sample types, most notably in that the gradient in the 3D spectrum is more gradual than that in the 2D spectrum in the VB region. These UPS spectra indicate that the electronic structure changes depending on the dimensionality of the material.

Figure 3 shows the total density of states (DOS) for the two crystals, as obtained by LCAO band calculations. The UPS spectra are shown for reference. The main component of the upper and lower VB's are I $5p$ orbitals and Pb $6p$ and I $5p$ orbitals, respectively, and the conduction band (CB) consists of Pb $6p$ and I $5p$ orbitals. The total DOS reveals that the VB and CB for the 3D crystal are constituted by widebands, whereas those for the 2D crystal consist of a number of localized bands.

The features of the calculated total DOS for the 3D and 2D crystals are in good agreement with the UPS spectra, the experimentally observed DOS. The observed peaks, $3A$, $3B$, and $2A$ to $2C$ are represented in the calculated total DOS. In both the 3D and 2D crystals, the two high-density bands ($3a_1$, $3a_2$ and $2a$, $2b$) are situated in the upper VB. Due to localization of electronic states in the direction of the *c* axis, the 2D crystal has sharper bands than the 3D crystal. The two

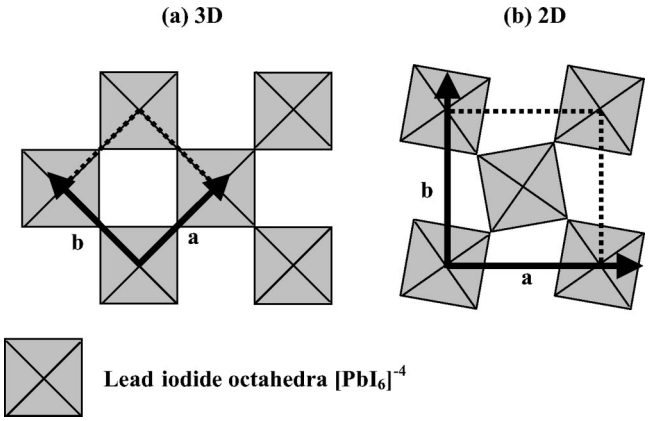

FIG. 5. Two-dimensional unit cells of (a) 3D crystal $CH_3NH_3PbI_3$ and (b) 2D crystal $(C_4H_9NH_3)_2PbI_4$ viewed along the *c* axis.

localized bands $2a$ and $2b$ appear as peaks 2A and 2B in the UPS spectra for the 2D crystal, while the two broad bands $3a_1$ and $3a_2$ in the 3D crystal are observed as one peak, $3A$. According to the preliminary calculations[23] in which the organic parts are considered, the bands due to the alkylammonium chains are situated in the middle of the VB (around $3b$ and $2c$). The bands of $CH_3NH_3^+$ and $C_4H_9NH_3^+$ were observed as the $3B$ and $2C$ peaks, respectively. The 3D crystal has a broader VB top than the 2D crystal due to the difference in bandwidth, as shown by the shaded areas in Figs. 2 and 3.

Based on the calculation results, the differences between the 3D and 2D crystals observed in the UPS spectra can be rationalized as due to a narrowing of bandwidth with decreasing dimensionality.

B. Energy-band structures

Figure 4 shows the energy-band structures of the 3D and 2D crystals according to LCAO band calculations along the high-symmetry *k* lines [see Figs. 4(c) and 4(d)]. The 3D and 2D crystals have a direct band gap at the *R* and Γ points, respectively. Figure 5 shows two-dimensional structures of both crystals, viewed down the *c* axis. As the 2D crystal has two formula units in the two-dimensional primitive cell, the bands are folded at the *X* and *Y* points [see Fig. 4(b)]. As previously mentioned, the 3D crystal has wider valence and conduction bands than the 2D crystal. Therefore, the band-gap energy increases with decreasing dimensionality. The calculated band-gap energies are 1.45 eV for the 3D crystal and 2.24 eV for the 2D crystal. The 1s exciton absorption peaks of the 3D and 2D crystals were observed at 1.65 eV and 2.44 eV, respectively.[24] The exciton binding energy from magneto-optical measurement studies is 45 meV for the 3D crystal[25] and 386 meV for the 2D crystal.[26] The experimental band-gap energies can then be estimated by adding the exciton binding energy to the exciton absorption energy: 3D, 1.70 eV; 2D, 2.83 eV. The band-gap energies calculated in the present study are much smaller than that experimentally observed due to the well-known shortcomings of the DFT.

Band calculations have shown that the bandwidth narrowing of the 2D crystal is attributable to the effect of decreasing dimensionality and structural distortion.

The effects of decreasing dimensionality can be seen in Fig. 4(b), where the band dispersions in the vertical directions (i.e., Γ-*Z* and *S*-*R*) are close to zero in the 2D crystal. This is the origin of the narrow bandwidth of the 2D crystal.

The structural distortion effects are shown in Figs. 5 and 6. The $[PbI_6]^{-4}$ octahedra of the 3D crystal forms orthogonal network with high symmetry (C_4), while the zigzag network of the 2D crystal has low symmetry (C_2). In order to examine the effect of structural distortion on the electronic structures of the 2D crystal, the energy-band structures were calculated for an ideal 2D crystal with C_4 symmetry and the same lattice constant as the 2D crystal. Figure 6 shows the energy-band structures of the ideal crystal and an actual $(C_4H_9NH_3)_2PbI_4$ 2D crystal along the Γ-*X* line. The VB and

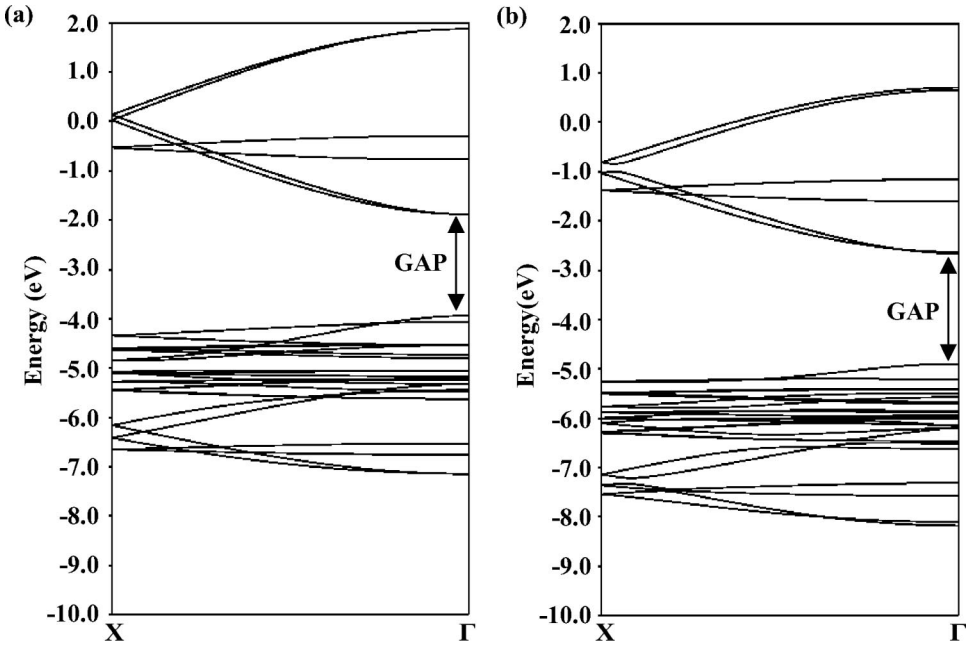

FIG. 6. Calculated band structures of (a) ideal and (b) actual 2D crystals along the Γ-*X* line. Ideal crystal has C4 symmetry and the same lattice constant as $(C_4H_9NH_3)_2PbI_4$, while the actual crystal is $(C_4H_9NH_3)_2PbI_4$ with C2 symmetry.

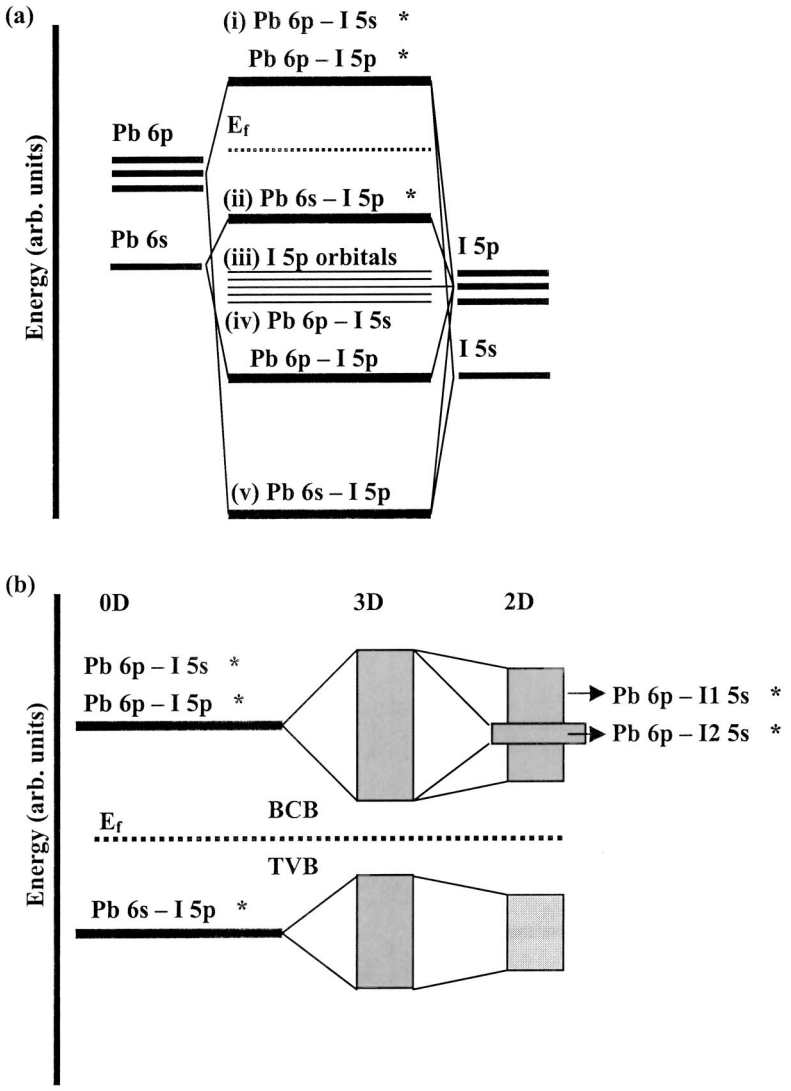

FIG. 7. Bonding diagram of (a) $[PbI6]^{-4}$ cluster (zero-dimensional system), (b) 3D crystal $CH_3NH_3PbI_3$, and (b) 2D crystal $(C_4H_9NH_3)_2PbI_4$ at the top of the valence band and the bottom of the conduction band.

CB of the actual 2D crystal are narrower and shifted to lower energies compared to those of the ideal crystal. This indicates that structural distortion and symmetry deterioration lead to bandwidth narrowing and energetic stability. This structural distortion effect is the well-known Jahn-Teller effect in a solid.[27]

The bandwidth narrowing is remarkable at the top of the VB (TVB) and bottom of the CB (BCB). The dispersions for the 2D crystal are smaller than for the 3D crystal near the TVB and BCB, resulting in a large effective mass of carriers, electrons, and holes. Therefore, it is reasonable to expect that the excitons have large binding energy in the 2D crystal. This explains the high stability and large binding energy of excitons in $(C_nH_{2n-1}NH_3)_2PbI_4$ as discussed in the previous papers, and also the dielectric confinement effect.[1–7,24–26]

C. Bonding mechanism

Figure 7(a) is a bonding diagram for the $[PbI_6]^{-4}$ cluster (zero-dimensional system). The lowest unoccupied states consist of Pb $6p$–I $5s$ σ-antibonding and Pb $6p$–I $5p$ π-antibonding orbitals. The higher occupied states can be decomposed into three parts: a Pb $6s$–I $5p$ σ-antibonding orbital in the top of the states, I $5p$ orbitals in the middle energy region, and Pb $6p$–I $5s$ σ-bonding and Pb $6p$–I $5p$ π-bonding orbitals in the bottom of the state. The Pb $6s$–I $5p$ σ-bonding orbital is situated in the lower-energy region. The local bonding scheme of the 3D and 2D crystals reflects the characteristics of the $[PbI_6]^{-4}$ molecule (0D). Figure 7(b) is the bonding diagram of the TVB and BCB for the 3D and 2D crystals. The TVB for the 3D crystal consists of the Pb $6s$–I $5p$ σ-antibonding orbital, while the Pb $6p$–I $5s$ σ-antibonding and Pb $6p$–I $5p$ π-antibonding orbitals form the BCB. In the 2D crystal, the I1 and I2 [see Fig. 1(b)] electronic orbitals are split in a two-dimensional ligand field. The TVB is composed of the Pb $6s$–I1 and I2 $5p$ σ-antibonding orbitals. The BCB of Pb $6p$–I1 $5s$ σ-antibonding and Pb $6p$–I1 $5p$ π-antibonding orbitals exhibits greater dispersion than the Pb $6p$–I2 $5s$ σ-antibonding band.

IV. CONCLUSIONS

The present study examined the electronic structures of the lead-iodide-based three-dimensional and two-dimensional OIPC's $CH_3NH_3PbI_3$ and $(C_4H_9NH_3)_2PbI_4$ by UPS and first-principles band calculations. The results obtained are summarized as follows.

(i) The differences between the VB electronic structures of $CH_3NH_3PbI_3$ and $(C_4H_9NH_3)_2PbI_4$ observed by UPS can be rationalized in terms of bandwidth narrowing with decreasing dimensionality.

(ii) Zero dispersion along the vertical direction and the Jahn-Teller effect in the layered structure cause bandwidth narrowing, resulting in small band dispersion of the TVB and BCB, a wideband gap and large binding energy of excitons in $(C_4H_9NH_3)_2PbI_4$.

(iii) The TVB and BCB of $CH_3NH_3PbI_3$ and $(C_4H_9NH_3)_2PbI_4$ are composed primarily of σ-antibonding states of Pb $6s$ and I $5p$ orbitals and σ-antibonding states of Pb $6p$ and I $5s$ orbitals, respectively.

ACKNOWLEDGMENTS

The authors are grateful to Associate Professor M. Rikukawa (Sophia University) for help with AFM measurements. This work was supported under the Sasagawa Scientific Research Grant from The Japan Science Society.

*Email address: tt17159@mail.ecc.u-tokyo.ac.jp.
†Email address: asai@q.t.u-tokyo.ac.jp.

[1] D.B. Mitzi, Prog. Inorg. Chem. **48**, 1 (1999).
[2] G.C. Papavassiliou, Prog. Solid State Chem. **25**, 125 (1997).
[3] T. Ishihara, *Optical Properties of Pb-based Inorganic-Organic Perovskite* (World Scientific, Singapore, 1995).
[4] M. Hirasawa, T. Ishihara, and T. Goto, J. Phys. Soc. Jpn. **63**, 3870 (1994).
[5] T. Ishihara, J. Takahashi, and T. Goto, Phys. Rev. B **42**, 11 099 (1990).
[6] T. Kataoka, T. Kondo, R. Ito, S. Sasaki, K. Uchida, and N. Miura, Phys. Rev. B **47**, 2010 (1993).
[7] E. Hanamura, N. Nagosa, M. Kumagai, and T. Takagahara, Mater. Sci. Eng. **1**, 255 (1988).
[8] G.C. Papavassiliou, Mol. Cryst. Liq. Cryst. Sci. Technol. Sect. **286**, 231 (1996).
[9] H.M. Whangbo and R. Hoffmann, J. Am. Chem. Soc. **100**, 5297 (1978).
[10] J.C. Slater, Phys. Rev. **81**, 385 (1952).
[11] V. R. Saunders, R. Dovesi, C. Rottei, M. Sausa, N. M. Harrison, R. Orlando, and C. M. Zicovich-Wilson, computer code CRYSTAL98 (University of Torino, Torino, 1998).
[12] W. Kohn and L.J. Sham, Phys. Rev. **140**, 1133 (1965).
[13] J.P. Perdew and Y. Wang, Phys. Rev. B **45**, 13244 (1992).
[14] A.D. Becke, Phys. Rev. A **38**, 3098 (1988).
[15] P. Durand and J.C. Bathelat, Theor. Chim. Acta **38**, 283 (1975).
[16] P.J. Hay and W.R. Wadt, J. Chem. Phys. **82**, 270 (1985).
[17] M. Nizam, Y. Bouteiller, B. Silvi, C. Pisani, M. Causa, and R. Dovesi, J. Phys. C **21**, 5351 (1988).
[18] K. Doll and H. Stoll, Phys. Rev. B **57**, 4327 (1998).
[19] A. Poglitsch and D. Weber, J. Phys. Chem. **87**, 6373 (1987).
[20] D.B. Mitzi, Chem. Mater. **8**, 791 (1996).
[21] D.B. Mitzi, C.A. Field, W.T.A. Harrison, and A.M. Guloy, Nature (London) **369**, 467 (1994).
[22] E.A. Muljarov, S.G. Tikhodeev, N.A. Gippius, and T. Ishihara, Phys. Rev. B **51**, 14 370 (1995).
[23] In the preliminary studies, the calculations were done using a model containing the organic parts, where the disordered $(C_nH_{2n-1}NH_3^+)$ chains with many different orientations were fixed in a certain position. Though this model can provide information about the contributions of the organic parts to the total DOS, it is difficult to determine the accurate band structures of the $[PbI_6]^{-4}$ networks because this has a lower symmetry when compared with the actual crystal.
[24] G.C. Papavassiliou and I.B. Koutselas, Synth. Met. **71**, 1713 (1995).
[25] T. Kataoka, T. Kondo, R. Ito, S. Sasaki, K. Uchida, and N. Miura, Physica B **184**, 132 (1993).
[26] M. Hirasawa, T. Ishihara, T. Goto, S. Sasaki, K. Uchida, and N. Miura, Physica B **201**, 427 (1994).
[27] L.E. Orgel and J.D. Dunitz, Nature (London) **179**, 462 (1975).